Organic & Biomolecular Chemistry

Accepted Manuscript

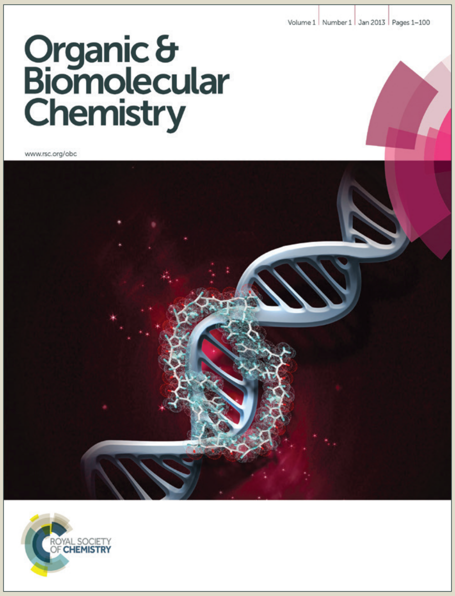

ROYAL SOCIETY OF CHEMISTRY

www.rsc.org/obc

Journal Name RSCPublishing

ARTICLE

Binding modes of a core-extended metalloporphyrin to Human Telomeric DNA G-quadruplexes

cias Cite this: DOI: 10.1039/x0xx00000x

Received XXth September 2014

DOI: 10.1039/x0xx00000x

www.rsc.org/

Jenifer Rubio-Magnieto,[a†] Florent Di Meo,[b†] Mamadou Lo,[c] Cécile Delcourt,[a] Sébastien Clément,[c] Patrick Norman,[b] Sébastien Richeter,*[c] Mathieu Linares,*[a,b] and Mathieu Surin*[a]

The molecular recognition of Human telomeric G-quadruplexes by a novel cationic π-extended Ni^{II}-porphyrin (Ni^{II}-**TImidP4**, Chart 1) is studied in aqueous solutions via (chir)optical spectroscopy, Fluorescence Resonance Energy Transfer (FRET) melting assay, and computational molecular modeling. The results are systematically compared to the recognition by a conventional *meso*-substituted Ni^{II}-porphyrin (Ni^{II}-**TMPyP4**, Chart 1), which allows us to pinpoint the differences in binding modes depending on the G-quadruplex topology. Importantly, FRET melting assays show the higher selectivity of Ni^{II}-**TImidP4** towards human telomeric G4 than that of Ni^{II}-**TMPyP4**.

Introduction

Specific guanine-rich oligonucleotides can fold or assemble into quadruplex structures, *i.e.* four guanines (G) form a square-planar network via Hoogsteen hydrogen-bonds, a G-quartet, and G-quartets can stack on top of each other stabilized by monovalent alkali cations such as potassium (K^+) or sodium (Na^+).[1-4] There is solid evidence that the human telomeric DNA sequence $d(TTAGGG)_n$ forms intramolecular G-quadruplexes at the end of chromosomes, and that G-quadruplexes are over-represented in promoter regions, such as oncogenes.[5-9] Therefore, G-quadruplexes have been identified as therapeutic targets, and the search for new molecules (ligands) that stabilize G-quadruplex topologies has become an active research field in anti-cancer drug design.[10-13] This includes organometallic complexes, planar aromatic structures, and macrocyclic ligands such as porphyrin derivatives.[14-17] Indeed, the structure and the photophysical properties of porphyrins make these compounds interesting for DNA recognition and sensing.[18-22] For instance, the tetrakis(*N*-methylpyridinium-4-yl)porphyrin (**TMPyP4**, see Chart 1 left, without metal center) can show different types of DNA binding modes, which depend of different factors such as the sequence and structure of DNA, the peripheral substituents on the porphyrin ring, and the composition of the solution.[23-26] If the porphyrin possesses a central metal (metalloporphyrin), the binding to G-quadruplexes depends on the nature of the metal: octahedral complexes (*e.g.* Co^{II} porphyrins, possessing axial ligands) bind externally to the G-quadruplex due to their 3D structure hindering intercalation in between G-quartets, whereas square-planar complexes (Cu^{II} or Ni^{II} porphyrins) can possibly intercalate in between G-quartets.[14,23,27]

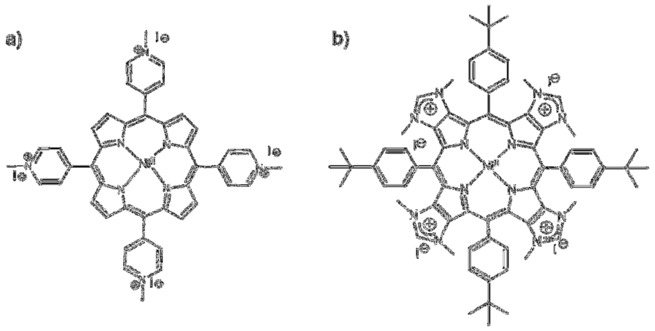

Chart 1 Chemical structures of the metalloporphyrins under study: (a) Ni^{II}-**TMPyP4** and (b) Ni^{II}-**TImidP4**.

Here, we describe the molecular recognition of intra-molecular G-quadruplexes (G4) by a metalloporphyrin Ni^{II}-**TImidP4** (Chart 1, right). Especially, we focus on human telomeric DNA sequences that form G4, here 22-mer and 30-mer oligonucleotides. These G4 sequences were identified as therapeutic targets, for which binding to a ligand, such as a porphyrin derivative, may inhibit telomerase, an over-expressed enzyme in 85-90% cancers.[13, 17, 28-30] In contrast to other metalloporphyrins studied so far for their interaction with

DNA, the four positive charges of Ni^{II}-**TImidP4** are located on the aromatic core of the porphyrin, *i.e.* on the fused imidazolium rings. The *meso* 4-*tert*-butylphenyl groups were used as solubilizing groups in the course of the synthesis of the corresponding tetraimidazole derivative in organic solvents.[31] However, these hydrophobic groups do not prevent Ni^{II}-**TImidP4** to be soluble in water. Keeping nickel(II) in the porphyrin was also a deliberate choice as we previously observed that free base porphyrins fused to imidazole rings may decompose before the quaternization reaction leading to the formation of Ni^{II}-**TImidP4**.[32] This expands the family of porphyrins to more π-extended cationic structures, for which the DNA G-quadruplexes recognition should be quite different due to the particular charge distribution and extended π-conjugated plane of this porphyrin. Our results are systematically compared to the recognition of human telomeric G4 to Ni^{II}-**TMPyP4** (Chart 1, left), for which the cationic substituents are placed in the four *meso* positions. Indeed, the porphyrin **TMPyP4** has been well-studied (with or without metal center) for its DNA-binding abilities, noticeably with G-quadruplexes.[10,19,23,33] We carry out UV-Vis spectroscopy and Circular Dichroism (CD) in aqueous solutions, which allow us to probe the G4/metalloporphyrin interactions as a function of the solution composition. Fluorescence Resonance Energy Transfer (FRET) melting assays provide valuable information into the stabilization and selectivity of the studied ligands towards G4. Molecular dynamics simulations are used to propose reliable supramolecular structures and to estimate binding free energies of the G4-porphyrin complexes. Finally, a comparison between CD experiments and computed chirality parameters support the identification of relevant binding modes.

Results and discussion

Synthesis of Ni^{II}-TImidP4

We have recently reported on the synthesis of π-extended porphyrin fused to imidazole rings across their β,β'-pyrrolic positions and showed that up to four imidazole rings could be fused to the aromatic core of the porphyrin (one on each pyrrole unit).[31] The tetrakis(imidazolium) salt Ni^{II}-**TImidP4** (see Chart 1, right) was obtained by alkylating the tetrakis(imidazole) derivative with an excess of iodomethane. The molecular mass peak of Ni^{II}-**TImidP4** was observed by ESI-TOF mass spectrometry at m/z = 292.6498, as expected for this tetracationic species (calculated m/z = 292.6496, see ESI Fig. S1 and S2). Ni^{II}-**TImidP4** is well soluble in protic polar solvents such as water (green solutions) and is very poorly soluble in organic solvents such as $CHCl_3$ (brown turbid solutions). The UV-visible spectrum of Ni^{II}-**TImidP4** in water showed that the Soret absorption band is broad and split with a main absorption band centred at λ = 436 nm and a shoulder on the right (Fig. S3 in ESI). This suggests that additional ligands (*i.e.* water molecules) are coordinated on the nickel center.[34] Moreover, the four imidazolium rings acting as electron deficient units also favour the coordination of axial ligands on the central nickel(II). Knowing that square pyramidal and distorted octahedral nickel(II) porphyrin complexes are paramagnetic (S = 1, high-spin), axial coordination of one and/or two molecule(s) of solvent on the nickel(II) center may explain the observed broad and split signals for Ni^{II}-**TImidP4** by ^{1}H NMR spectroscopy in d^6-methanol (Fig. S4 in ESI). This is confirmed by the fact that the same phenomenon was observed with the porphyrin fused to three imidazolium rings in d^6-methanol, while sharp and well-defined signals were observed for this compound in a non-coordinating solvent like $CDCl_3$ (Fig. S5 in ESI).

Binding to Human Telomeric Sequences

The human telomeric sequence d(TTAGGG)$_n$ can adopt different intramolecular G-quadruplex structures with backbone loop-shapes depending on the aqueous solution conditions, especially on the nature of the salt.[35-37] Human telomeric G-quadruplexes possess a large structural diversity, as recently reviewed.[38] The main human telomeric sequence studied here d[$AG_3(T_2AG_3)_3$], hereafter referred to as **Tel22**, presents parallel and/or anti-parallel G4 loop structure depending on the alkali cation in aqueous solution. In solutions of potassium ions (K$^+$), this sequence forms a mixture of parallel and anti-parallel G-quadruplex conformations, in a dynamic equilibrium between hybrid structures.[35,39-41] This is observed using circular dichroism (CD) experiments, showing a CD spectrum characterized by positive maximum at 290 nm, a plateau at 265 nm, and a negative peak at 240 nm (Fig. 1 and Fig.S7 in ESI).

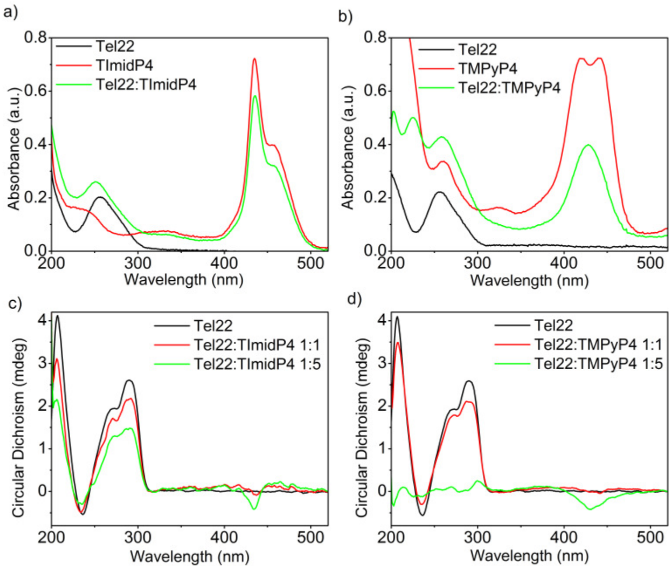

Fig. 1 UV-Vis (top) and CD spectra (bottom) of a) and c) Tel22: Ni^{II}-**TImidP4** 1:N and b) and d) Tel22:Ni^{II}-**TMPyP4** 1:N in TE buffer + 100 mM KCl. The molar ratio for a) and b) is 1:5.

In the presence of sodium ions (Na$^+$), **Tel22** presents an anti-parallel "basket-type" structure, with a characteristic positive peak at 295 nm and an intense negative peak at 260 nm (Fig. 2 and Fig. S7 in ESI).[37] The molecular recognition of **Tel22** to each metalloporphyrin was studied in different solution conditions using CD and UV-Vis absorption. Figure 1c shows the CD spectra of **Tel22**:Ni^{II}-**TImidP4** mixtures in a aqueous solution containing 100 mM KCl. The typical CD signal of this telomeric hybrid G4 structure in K$^+$ solution, *i.e.* a positive peak at 290 nm and a plateau at 265 nm, is maintained whatever the molar ratio. Moreover, we observe a weak negative induced CD signal (ICD) in the Soret band of the metalloporphyrin, which increases at 1:5 molar ratio. This indeed suggests that Ni^{II}-**TImidP4** interacts with **Tel22**. In contrast, for mixtures of **Tel22**:Ni^{II}-**TMPyP4** (Fig. 1d), no ICD is observed at 1:1 molar ratio, and at a molar ratio of 1:5 a weak negative ICD is observed but the CD signal of **Tel22** (200-320 nm) has completely vanished. This is in agreement with other studies showing that the porphyrin **TMPyP4** can unfold G-quadruplex structures.[42,43] The CD spectra indicates that the core-extended metalloporphyrin Ni^{II}-**TImidP4** stabilizes the initial G4 conformations of **Tel22** in presence of K$^+$, while the binding to (an excess of) Ni^{II}-**TMPyP4** may lead to unfolding of the G-quadruplex conformations. This is likely due to the stronger intermolecular interactions of Ni^{II}-**TMPyP4** with DNA bases (see below).

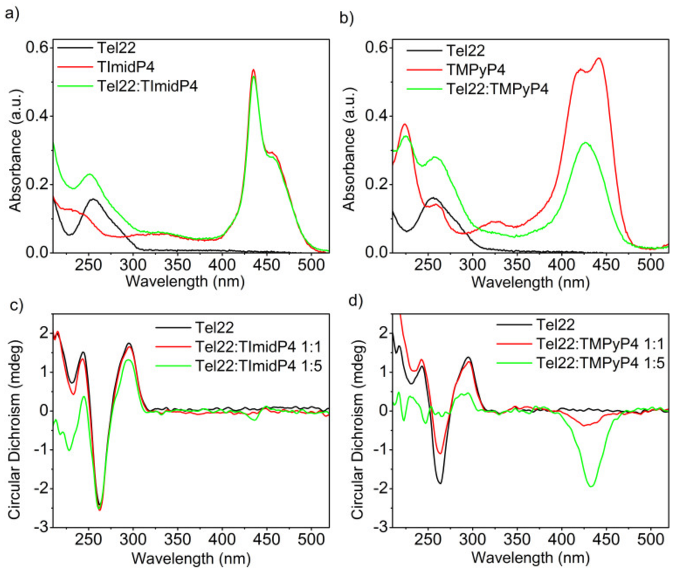

Fig. 2 UV-Vis (top) and CD spectra (bottom) of a) and c) Tel22: Ni^{II}-**TImidP4** 1:N and b) and d) Tel22:Ni^{II}-**TMPyP4** 1:N in TE buffer + 100 mM NaCl. The molar ratio for a) and b) is 1:5.

This is supported by UV-Vis absorption spectra shown in Figs. 1a-b. Pure Ni^{II}-**TMPyP4** shows two overlapping bands in the Soret region: one at 420 nm due to the diamagnetic four-coordinate form and one at 441 nm due to the paramagnetic diaquo complex (Fig. 1b). Upon interaction with **Tel22**, the UV-Vis spectrum shows a red-shifted absorption maximum ($\Delta\lambda_{max}$ ~ 8 nm) and a large hypochromicity in the Soret band. This is different for Ni^{II}-**TImidP4**, for which UV-Vis spectra show no change in the shape and a smaller hypochromicity in the Soret band upon binding to **Tel22** (Fig. 1a). As indicated above, a shoulder is noticed on the right which may indicate that one or two ligands (*i.e.* water molecules) are coordinated on the nickel center.[34]

For each metalloporphyrin, the same types of changes in spectra were observed upon binding to the longer human telomeric sequence **Tel30** (d[GT$_2$A(GGGTTA)$_4$GG]), a sequence also presenting a mixture of anti-parallel and parallel G4 conformations in KCl solutions (Fig. S8 in ESI). This indicates that larger G-quadruplexes structures have rather identical recognition modes by these metalloporphyrins.

In aqueous solutions containing 100 mM NaCl, the **Tel22** adopts an anti-parallel G-quadruplex conformation. As observed in the CD spectra shown in Fig. 2c, this anti-parallel G4 conformation is maintained upon addition of Ni^{II}-**TImidP4** metalloporphyrin. No ICD in the Soret band is observed at 1:1 molar ratio, and only a weak ICD signal is observed with 5 equivalents of Ni^{II}-**TImidP4**. In contrast, upon addition of Ni^{II}-**TMPyP4** metalloporphyrin, at a 1:1 molar ratio, an ICD is observed in the Soret band, and at 1:5 the CD signals characteristic for the G4 structure **Tel22** starts to vanish (Fig. 2d and Fig. S9). The negative ICD signal is much more pronounced for the **Tel22**:Ni^{II}-**TMPyP4** mixture. This signal notably differs to what happens with Zn^{II}-**TMPyP4** octahedral complex, yielding a bisignated ICD peak, which was ascribed to an end-stacking binding mode.[44] The difference in binding modes to **Tel22** between Ni^{II}-**TMPyP4** to Ni^{II}-**TImidP4** can be ascribed to the extended π-conjugated system and the saddle conformation of Ni^{II}-**TImidP4**, as discussed here below. Again, the UV-Vis experiments are consistent with ICD signals in that they show that, upon interaction with **Tel22**, the Ni^{II}-**TMPyP4** shows larger perturbations in the Soret band than for Ni^{II}-**TImidP4** (Figs. 2a-b).

In order to assess the binding properties of Ni^{II}-**TImidP4** towards **Tel22**, a FRET melting assays were performed, as this is a valuable method to assess the stabilization and selectivity of G4 ligands.[45, 46] This method is based on the measurement of melting properties of a double-dye labelled oligonucleotide, as followed by fluorescence spectra showing FRET between the two dyes when the oligonucleotide is folded in G4 conformation. Here we used a modified human telomeric sequence end-capped with a fluorescein amidite dye (FAM) at 5'-end and a tetramethylrhodamine (TAMRA) at 3'-end, this labelled oligonucleotide FAM-5'-GGG(T$_2$AG$_3$)$_3$-TAMRA-3' being named **F21T** being widely studied in literature for G4-ligand studies. After a preliminary heating/cooling cycle of **F21T**, we added the studied porphyrin and followed the emission of the donor dye (*i.e.* FAM) as a function of temperature. This method has been shown to give more reproducible results than the sensitized emission of the acceptor (*i.e.* TAMRA).[45] The G4 structure unfolds when the temperature increases and thereby the fluorescence emission of FAM occurs. This denaturation can be followed by plotting melting curves, which show the increase in FAM fluorescence as a function of temperature for pure **F21T** and for the mixtures **F21T**/Ni^{II}-**TImidP4** and **F21T**/Ni^{II}-**TMPyP4** at 1:5 molar ratio in a K$^+$ buffer conditions (Fig. 3a). The determination of the half-melting temperature difference ($\Delta T_{1/2}$) between the pure oligonucleotide and the same oligonucleotide bound to a ligand, is a quantitative analysis of the stabilization effect induced by the ligand (Fig. 3b). The results show that the $\Delta T_{1/2}$ is around 25 °C and around 23 °C for **F21T**/Ni^{II}-**TImidP4** and **F21T**/Ni^{II}-**TMPyP4**, respectively (Fig. 3). The latter value is in agreement with the one obtained by Romera *et al.*, who studied the influence of the incorporation of a metal ion on the G4-binding properties of TMPyP4 porphyrin.[27] Thus, the π-extended metalloporphyrin Ni^{II}-**TImidP4** could be considered as a good G4-ligand, as it induces an increase the melting temperature of **F21T** close or slightly higher than in the case of other well-considered G-quadruplex ligands.[47]

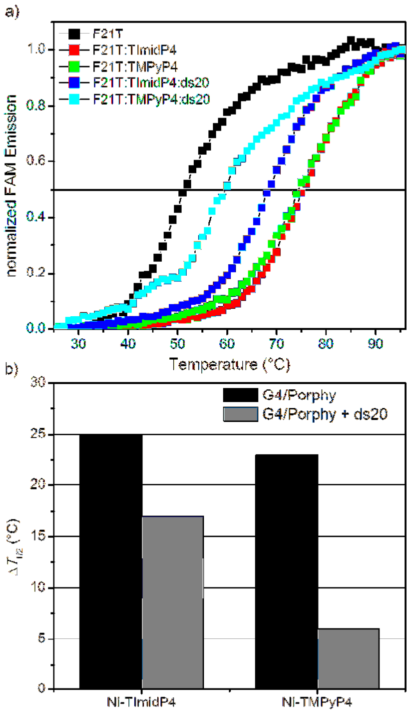

Fig. 3 a) Melting curves of 200 nM pure F21T and in the presence of 1 µM Ni^{II}-**TImidP4** ligand or 1 µM Ni^{II}-**TMPyP4** ligand without or with the presence of 15 equiv. of competitor double-stranded DNA (ds20). The curves shown correspond to normalized FAM fluorescence. b) Melting temperature differences $\Delta T_{1/2}$ from the FRET melting assays for each metalloporphyrin without and with the presence of the competitor **ds20**. All measurements were performed in a 10 mM lithium cacodylate buffer (pH = 7.2) with 10 mM KCl and 90 mM LiCl.

In order to evaluate the selectivity of this ligand, a competitor double-stranded DNA **ds20** (oligonucleotide 5'-CGTCACGTAAATCGGTTAAC-3' hybridized with its complementary sequence), was added to the **F21T**/Ni^{II}-**TImidP4** and F21T/Ni^{II}-**TMPyP4** complexes in an excess of 15 equivalents as compared to **F21T**. The decrease in $\Delta T_{1/2}$ shows that the Ni^{II}-**TImidP4** ligand is affected by the presence of the **ds20** competitor; however this decrease is more pronounced for the Ni^{II}-**TMPyP4** (Fig. 3b). Therefore, the core-extended metalloporphyrin Ni^{II}-**TImidP4** showed a higher selectivity for G-quadruplex DNA than the conventional Ni^{II}-**TMPyP4**.

Supramolecular structures of Ni^{II}-porphyrin – Tel22 complexes

Molecular dynamics (MD) simulations were carried out to give insights into the structures and binding modes of the studied porphyrins to model intramolecular G4: anti-parallel "basket-type" G4 (with Na$^+$, PDB ID: 143D), parallel G4 (with K$^+$, PDB ID: 1KF1) and hybrid G4 (mixed parallel/anti-parallel strands, PDB ID: 2HY9) structures of **Tel22**.[37, 41, 48] Only 1:1 complexes were considered for the sake of computational cost, taking into account the water explicitly (TIP3P model). MD simulations were carried out on a 100 ns timescale, allowing us to explore the movements of a single porphyrin around each G4 type and the possible interactions sites. Five starting conformations were considered, as depicted in Fig. 4.

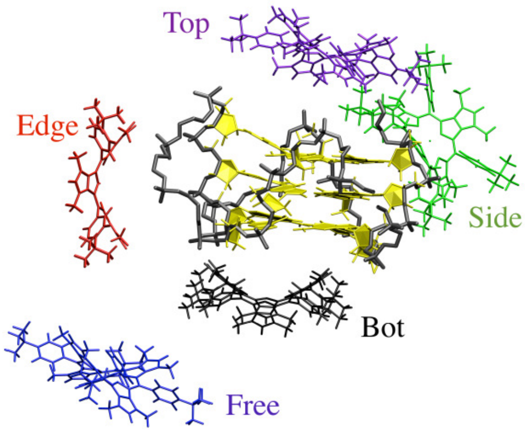

Fig 4 View of the initial conformations of 1:1 Ni^{II}-**TImidP4** – parallel Tel22 complexes for MD simulations. The guanosines are depicted in yellow (T and A bases are omitted for clarity), the phosphate backbone is depicted as a grey tube. The porphyrin is depicted in black, red, blue, green or violet depending on the considered conformation.

Ni^{II}-TImidP4 – G4 complexes.

Ni^{II}-**TImidP4** has a peculiar non-planar saddle shape conformation of the porphyrin macrocycle, as shown in Fig. 4. This is in accordance with (*i*) the crystal structure of a porphyrin fused to two imidazole rings which is also saddle shaped,[31] and (*ii*) with experimental evidences and modeling studies showing that highly substituted porphyrins adopt very distorted non-planar conformations, including saddle shape distortion.[49]

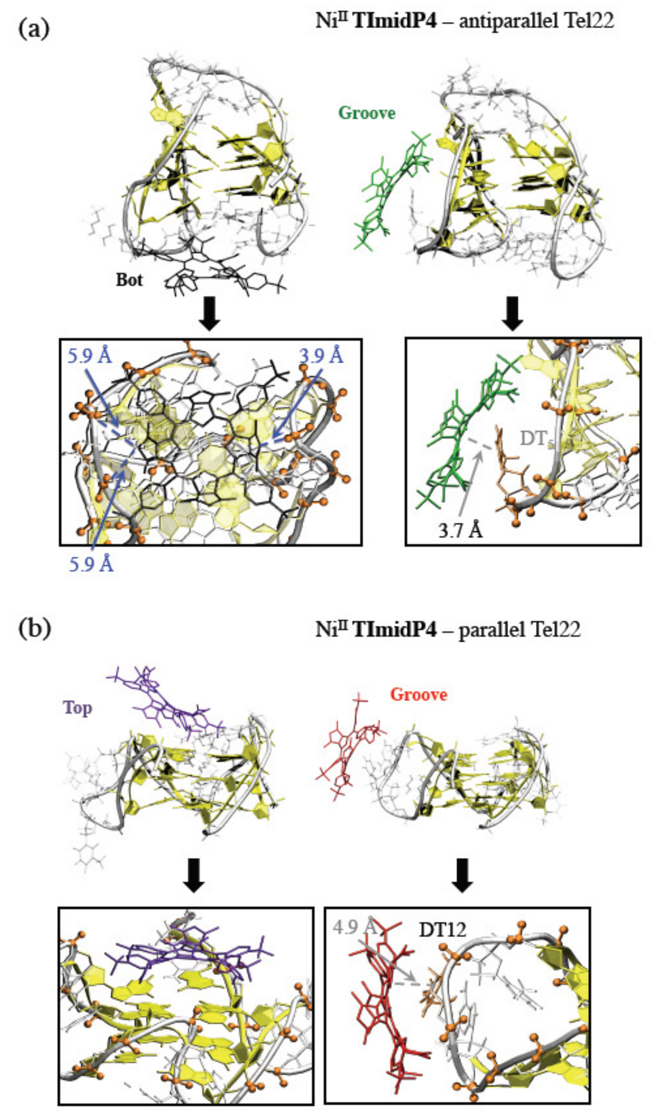

Fig. 5 Conformations and zooms of a representative snapshots at the end of MD simulations of 1:1 Ni^{II}-**TImidP4** complex with (a) anti-parallel and (b) parallel G-quadruplexes. Porphyrins are coloured by binding mode (*i.e.*, bot, top, and groove in black, violet and red/green, respectively). Relevant phosphates, residues are depicted in orange. Relevant distances involving electrostatic and van der Waals interactions are depicted in blue and grey, respectively.

Out of the five starting conformations of this porphyrin in interaction with the anti-parallel G-quadruplex, the outcome of Out of the five starting conformations, MD runs reveals two preferential binding modes, namely Bot and Groove conformations, see Fig. 5 and Fig. S10 and Table S1 in ESI. In the Bot conformation, the saddle shape of Ni^{II}-**TImidP4** perfectly accommodates the d(TTA) loop structure (Fig. 5a). The imidazolium groups strongly interact with negatively-charged phosphate groups due to electrostatic interactions. Interestingly, the binding occurs on both facing imidazolium moieties with the two bottom d(TTA) loops. The π-stacking interactions between G-quartet and Ni^{II}-**TImidP4** are expected to be weak since the saddle shape of the porphyrin together with the specific d(TTA) loop structure of this anti-parallel G4, covering the G-quartets. Note that different side-groove binding modes are observed (Fig. S10 in ESI), for which Ni^{II}-**TImidP4** is nested in the wide grooves of the anti-parallel G4, as for other organometallic complexes.[50]

Three preferential binding modes are also obtained for Ni^{II}-**TImidP4** – parallel G-quadruplex complexes, namely Bot, Top and Groove, see Fig. 5b and Fig. S10. In contrast to interactions with anti-parallel G4, Top conformations are accessible since the loops do not cover the G-quartets in this structure. The Groove binding mode is comparable to the one with anti-parallel G4, the imidazolium interacting here with dT12 (Fig. 4b). Note that MD simulations starting from hybrid parallel/anti-parallel G4 folding (PDB ID: 2HY9) yields the same preferential binding modes (Bot, Top Groove). In this case the Bot conformation show π-stacking between Ni^{II}-**TImidP4** and 3'-terminal adenine (Fig. S11).

*Ni^{II}-**TMPyP4** – G4 complexes.*

Ni^{II}-**TMPyP4** possesses a planar central porphyrin macrocycle, in strong contrast to the saddle shape of Ni^{II}-**TImidP4**. Furthermore, the cationic pyridinium moieties are located at the four *meso* positions (Chart 1) while for Ni^{II}-**TImidP4** the imidazolium moieties are fused to the β-pyrrolic positions, which lead to different G4 binding modes from MD simulations (Fig. 6 and Fig. S12). Interestingly, the Bot binding conformation consists in the perpendicular approach of the porphyrin with respect to the anti-parallel G4 (Fig. 5a), via electrostatic interactions between phosphate backbone and pyridinium moieties (ca. 4.5 Å) and π-stacking interactions with thymine in the loop (dT6). A side-groove binding mode is also observed, for which three pyridinium moieties interact with G4 phosphate groups through electrostatic interactions.

For complexes with the parallel G4 structure (Fig. 6b), the G-quartets are uncovered, solvent-accessible, which allows the planar structure of Ni^{II}-**TMPyP4** to interact via π-stacking interactions. Such interactions allow both stable Bot and Top supramolecular complexes in which this porphyrin is also electrostatically anchored to phosphate groups (Fig. 6b). Note that side-groove supramolecular complexes are also observed, in which Ni^{II}-**TMPyP4** is anchored to backbone phosphates through electrostatic interactions (Fig. S12).

Table 1 Binding energies for 1:1 complexes of Ni^{II}-**TImidP4** (a) or Ni^{II}-**TMPyP4** (b) – anti-parallel or parallel G-quadruplexes estimated from 100ns MD simulations. The non-covalent binding energies are decomposed in electrostatic and van der Waals contributions (E_{elec}, E_{vdw}, in kcal.mol^{-1}) and the relative binding free energies are computed in MM-GBSA approach ($\Delta\Delta G_{MM\text{-}GBSA}$, kcal.mol^{-1}).

a) Ni^{II}-**TImidP4** Conformation	Anti-parallel G-quadruplex				Parallel G-quadruplex		
	E_{elec}	E_{vdW}	$\Delta\Delta G_{MM\text{-}GBSA}$		E_{elec}	E_{vdw}	$\Delta\Delta G_{MM\text{-}GBSA}$
Bot	-166.1	-46.9	0.0	Bot	-115.7	-28.5	+11.5
Groove A	-112.7	-32.4	0.0	Top	-135.7	-37.2	0.0
Groove B	-87.6	-19.6	+9.0	Groove	-124.8	-24.6	+9.4

b) Ni^{II}-**TMPyP4** Conformation	Anti-parallel G-quadruplex				Parallel G-quadruplex		
	E_{elec}	E_{vdW}	$\Delta\Delta G_{MM\text{-}GBSA}$		E_{elec}	E_{vdw}	$\Delta\Delta G_{MM\text{-}GBSA}$
Bot	-172.1	-30.5	+10.0	Bot	-196.3	-42.6	0.0
Top	-124.1	-24.1	+13.1	Top	-178.8	-43.0	+5.4
Groove	-194.0	-32.0	0.0	Groove	-155.7	-28.3	+15.6

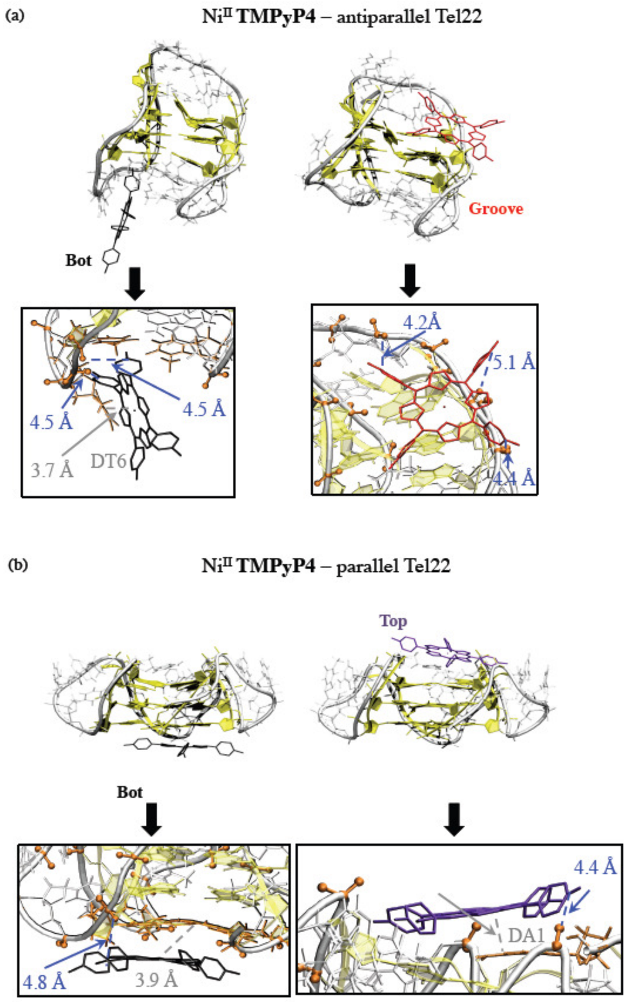

Fig. 6 Conformations and zooms of representative final snapshots from 100 ns MD simulations of 1:1 Ni^{II}-**TMPyP4** with (a) anti-parallel and (b) parallel G-quadruplexes. Porphyrins are coloured by binding mode (*i.e.*, bot, top, and groove in black, violet and red, respectively). Relevant phosphates groups are coloured in orange. Relevant distances involving predicted electrostatic and van der Waals interactions are depicted in blue and grey, respectively.

Binding energies in Ni^{II}-porphyrin – Tel22 complexes

To assess the preferential binding modes over the conformation obtained by MD, binding free energies ($\Delta\Delta G_{MM\text{-}GBSA}$, Table 1) for each porphyrin-G4 complex are estimated and are rationalized by calculating electrostatic and van der Waals energy contributions along MD runs, see Table 1. Although electrostatic contributions play a major role, the van der Waals interactions cannot be neglected since they significantly contribute to the total non-covalent interactions energy E_{nc} ($E_{nc} = E_{elec} + E_{vdw}$). For example, in the Bot conformation of Ni^{II}-**TImidP4** with anti-parallel G-quadruplex, it must be stressed that strong electrostatic contribution are in line with strong van der Waals contribution (Table 1a), because this porphyrin is anchored to G4 by both electrostatic interactions and π-stacking interactions with loop nucleobases (Fig. 5a).

By analysing the estimates of the relative binding free energies ($\Delta\Delta G_{MM\text{-}GBSA}$), both Ni^{II}-porphyrins preferentially bind to the anti-parallel G-quadruplexes in Bot or Groove conformations, respectively ($\Delta\Delta G_{MM\text{-}GBSA} = 0$ being by definition the most stable structure calculated for each type of complex), which are therefore the most likely conformations in Na^+ solutions. Note that the binding free energy for Bot or Groove A conformations of Ni^{II}-**TImidP4** with anti-parallel G4 is in the same range, while electrostatic and van der Waals contributions are significantly lower in Groove A. This can be rationalized by a lower destabilization of the G4 internal structure.

However, the preferential binding modes of the two studied porphyrins with parallel G4 are different. For Ni^{II}-**TImidP4**, the Top conformation is the most stable one, with a partial overlap of the aromatic core to the top G-quartet. The same Top preferential binding mode is obtained for conformations with the hybrid parallel/anti-parallel G4 (see Fig. S11), which altogether indicate that this is likely the preferential binding mode for Ni^{II}-**TImidP4–Tel22** in K^+ solutions. In contrast, the Bot is the preferential conformation for Ni^{II}-**TMPyP4**. In this case, the total non-covalent interactions are the strongest, because the core of the porphyrin is fully adsorbed, π-stacked to a G-quartet, while the four pyridinium groups accommodate close to DNA phosphate groups. This is in line with experimental CD spectra, showing the highest ICD signals for this mixture at a 1:1 molar ratio, whereas almost no ICD is observed for Ni^{II}-**TImidP4** in the same conditions. Note that the Bot and Top binding modes would allow an intercalative binding mode for 1:2 porphyrin – G4 complexes; in which a porphyrin would be located in between two G-quartets structures, as suggested in the literature.[51]

Binding modes and (chir)optical properties

Both Ni^{II}-**TMPyP4** and Ni^{II}-**TImidP4** inherently exhibit C_{2v} symmetry. These molecules are achiral and are CD-silent in the aqueous solution conditions used here (see Fig. S13 in ESI). However, the electrostatic and π-stacking interactions with G-quadruplexes induces geometrical deformations that can break the inherent central symmetry of porphyrins. This is what is observed by induced CD (ICD) signals reported here. Indeed, for specific mixtures our experiments exhibit a weak negative ICD band around 435 nm, *i.e.* in the Soret band of the metalloporphyrin, assigned to a π-π* transition on the tetrapyrrole moiety. In view of correlating the ICD signals with binding modes, the geometrical deformations were assessed from MD simulations, and the chirality parameters were estimated, see Fig 7.

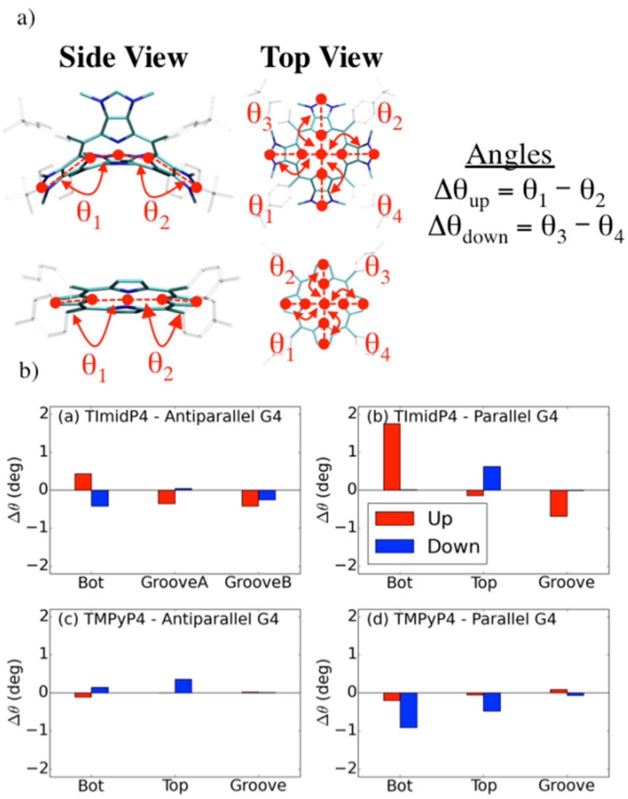

Fig. 7 a) Geometrical parameters assessing induced chirality of porphyrins. "Up" and "Down" annotations refer to side in contact or not with G-quadruplex, respectively. Only one example of pair angle is shown on the side view for the sake of clarity. b) Averaged chirality parameters $\Delta\theta_{down}$, $\Delta\theta_{up}$ for the last 10 ns MD simulations of (a) Ni^{II}-**TImidP4** with anti-parallel G4 and (b) parallel G4 and (c) Ni^{II}-**TMPyP4** with anti-parallel G4 and (d) parallel G4.

We focus on specific geometrical parameters of Ni^{II}-**TImidP4**: the angles $\theta_{1,2,3,4}$ formed by the Ni-atom, the N-atom of the pyrrole units and the corresponding CH-imidazolium moieties (Fig. 7a). For Ni^{II}-**TMPyP4**, the geometrical parameters are defined as the angles formed by the Ni-atoms, the N-atom of the pyrrole units and the centres of mass of the corresponding pyrrole C-C bonds. $\Delta\theta_{up}$ and $\Delta\theta_{down}$ are defined as the angle differences between each facing angle (for example, $\theta_1 - \theta_2$ and $\theta_3 - \theta_4$). The "Up" annotation refers to the side in close contact with the G-quadruplex along MD runs. An ICD signal in the Soret region is observed if and only if each parameter is nonzero. The chirality parameters are shown in Fig. 7b, as estimated for the various binding modes obtained at the end of MD simulations depicted in Figs. 5-6.

The chirality parameters of Ni^{II}-**TImidP4** metalloporphyrin upon interaction with **Tel22** are higher when it interacts with the parallel or hybrid G4 (*i.e.* structures relevant to K^+ solutions) than with the anti-parallel G4 (*i.e.* structures relevant to Na^+ solutions), see Fig. 7b and Fig. S11. Indeed, in the anti-parallel G4, the d(TTA) loops surround the Top and Bottom faces of the G-quartets, yielding a globular shape, which makes easier for curved-aromatic porphyrin Ni^{II}-**TImidP4** to be nested in a wide Groove, leading to minute conformational change on this metalloporphyrin. This is in fair agreement experimental CD shown in Figs. 1 and 2: the ICD signals of this metalloporphyrin are very weak in presence of NaCl (*i.e.*, anti-parallel conformation) and only appear at a 1:5 molar ratio.

Besides, the averaged chirality parameters Δθ for Ni^{II}-**TMPyP4**:**Tel22** are slightly lower than for Ni^{II}-**TImidP4**:**Tel22** (Fig. 6b), *i.e.* the planar tetrapyrrole is less deformed upon interaction with G4. However, the deformation of the core is not the only parameter influencing the chirality of the molecule. Indeed the rotation of the rings in *meso* position can also affect the CD response. For **TImidP4**, the rotation is locked and only the deformation of the core is possible, while for **TMPyP4** the relative orientation of the pyridinium groups can also induce chirality.

Conclusions

The recognition modes of a new cationic π-extended metalloporphyrin Ni^{II}-**TImidP4** towards Human telomeric G-quadruplexes have been studied. By comparing (chir)optical spectroscopy and MD simulations, we have revealed the differences in preferential binding modes with respect to a conventional *meso*-substituted Ni^{II}-**TMPyP4**. We show that Ni^{II}-**TImidP4** maintains both anti-parallel and parallel G4 conformations up to 5 equivalents of **Tel22**. Importantly, FRET melting assays show the higher stabilization and selectivity of Ni^{II}-**TImidP4** towards human telomeric G4 than with the conventional Ni^{II}-**TMPyP4**. These results can have significant implications in the context of G4 as therapeutic targets.

Experimental

General experimental

Reagents and solvents were purchased from commercial suppliers (Aldrich, Fluka, or Merck) and were used without further purification. The oligonucleotides (ODN) were purchased from Eurogentec (Belgium) with the highest purity grade (UltraPure Gold^{TM}, > 95% pure in sequence) in dried state, and the purity of the ODN sequences was checked with MALDI-ToF.

Synthetic procedures

General procedure for synthesis of Ni^{II}-**TimidP4**. The corresponding porphyrin fused to four imidazoles was used as starting material and its synthesis was previously reported by one of us.[31] The porphyrin fused to four imidazoles (18 mg, 0.0107×10^{-3} mmol) was dissolved in DMF (5 mL) and an excess of iodomethane (1 mL), was added. The reaction mixture was vigorously stirred under an atmosphere of argon for 48 hours. Then, the excess of iodomethane and the DMF were evaporated under reduced pressure to leave the crude product which was purified by column chromatography on alumina ($CHCl_3$ + 2% MeOH). The solvents were evaporated and Ni^{II}-**TImidP4** was obtained in 56% yield (16 mg). ^{1}H NMR (300 MHz, CD_3OD, 25°C): δ = 2.69 (s, tBu), 3.96 (s br., NCH_3), 8.00-9.80 (m, Hmeso + C-Himidazolium) ppm. ^{13}C NMR (151 MHz, CD_3OD, 25°C): δ = 33.2, 35.4, 44.7, 64.9, 101.4, 130.2, 160.0, 177.3 ppm. HR ESI-TOF$^+$ MS: *m/z* calcd. for $NiC_{72}H_{80}N_{12}{}^{4+}$: 292.6496 $[M - 4I]^{4+}$; found: 292.6498. UV/Vis (H_2O): λ_{max} (ε) = 436 (134500), 458 sh (70300), 548 (5400), 592 (9700), 639 nm (10100 L.mol^{-1}.cm^{-1}).

General procedure for synthesis of Ni^{II}-**TMPyP4**. The corresponding nickel(II) porphyrin bearing four pyridyl groups in *meso* positions was obtained following a previously reported synthetic procedure.[52] Alkylation of this compound following the same protocol for the synthesis of Ni^{II}-**TImidP4** afforded Ni^{II}-**TMPyP4**.[53]

Preparation of the porphyrin-G4 mixtures

The buffer was prepared by using tris(hydroxymethyl) aminomethane ($(HOCH_2)_3CNH_2$), EDTA and Milli-Q water. The oligonucleotides were dissolved in a volume of TE buffer (pH 7.4, 10 mM Tris buffer and 1mM EDTA) at a concentration of 100 µM. All ODN solutions obtained were centrifuged during 2 minutes at 2000 rpm. Small volumes of this solution were used in order to prepare different aliquots, on which were added TE buffer, or TE buffer + KCl 3M or + NaCl 3M in order to obtain a final volume of 300 µL and solutions in pure TE buffer or TE buffer + 100 mM K$^+$ ions or TE buffer + 100 mM Na$^+$ ions, respectively. The final solution was mixed using a vortex. The concentration of the aliquot of DNA in the buffer solution was determined by UV-Vis at 25 ºC using the specific extinction coefficients at 260 nm (ε_{260}) of each DNA, which are 228500 L.mol^{-1}.cm^{-1} and 306900 L.mol^{-1}.cm^{-1}, for **Tel22** (d[$AG_3(T_2AG_3)_3$]) and **Tel30** (d[$GT_2A(GGGTTA)_4GG$]), respectively. The Ni^{II}-porphyrins samples were also dissolved in TE buffer (pH 7.4, 10 mM Tris buffer and 1 mM EDTA) or in TE buffer + 100 mM KCl or NaCl and the molar ratio between metalloporphyrins and DNA was adjusted using the calculated molar concentrations of DNA (around 3.5 µM). The molar extinction coefficient (ε) for Ni^{II}-**TMPyP4** at 418 nm is 149000 L.mol^{-1}.cm^{-1} and for Ni^{II}-**TImidP4** is 134500 L.mol^{-1}.cm^{-1} at 436 nm. The solution of metalloporphyrin was added to the DNA solution and was stirred using a vortex at vigorous speed during 2 min. and allowed to equilibrate for 30 min.

UV-Vis absorption and Circular Dichroism spectroscopy

The UV-Vis absorption and circular dichroism (CD) measurements were recorded using a Chirascan^{TM} Plus CD Spectrometer from Applied Photophysics. The measurements were carried out using 1 mm suprasil quartz cells from Hellma Analytics. The spectra were recorded between 200 and 650 nm, with a bandwidth of 1 nm, time per point 1 s and 2 repetitions. The buffered water solvent reference spectra were used as baselines and were automatically subtracted from the CD spectra of the samples.

FRET melting assays

Fluorescence resonance energy transfer (FRET) melting assays were performed according to Mergny et *al.*[45], using a synthetic double-dye labelled oligonucleotide **F21T** 5'-FAM-GGG(T_2AG_3)$_3$-TAMRA-3' (from Eurogentec, Belgium). The solutions were prepared at a concentration of around 200 nM (base concentration) in 10 mM lithium cacodylate buffer (pH = 7.2) in presence of 10 mM KCl + 90 mM LiCl (K$^+$ medium). The oligonucleotide was first heated to 90 ºC for 3 min in the corresponding buffer conditions and then put on ice to support the formation of G4 secondary structure. The metalloporphyrin was then added at a concentration of ~ 1 µM, and the mixture was equilibrated at 25 ºC during 5 minutes. The FRET spectra were measured using a Chirascan^{TM} Plus instrument equipped for fluorescence measurements. The samples were excited at 492 nm and the fluorescence emission spectra were collected between 500 and 700 nm. The temperature was varied from 25 ºC to 96 ºC at a rate of 1 ºC/min. The melting of the **F21T** was monitored by measuring the fluorescence of FAM (at 516 nm), as described in reference [45]. The FAM emission intensity was normalized and $\Delta T_{1/2}$ was defined as the temperature for which the normalized emission equals 0.5. For the selectivity studies, a solution of 15 equivalents of a dsDNA competitor (~ 3 µM) was added into the **F21T**/metalloporphyrin solution and the final solution was equilibrated at 25 ºC during 5 minutes. The dsDNA competitor is 5'-CGTCACGTAAATCGGTTAAC-3' hybridized with its complementary sequence.

Molecular modeling simulations

Force Field parameterization. Force field parameters of Ni^{II}-**TMPyP4** and Ni^{II}-**TImidP4** metalloporphyrins were derived from GAFF[54] and quantum mechanics calculations at the (*IEFPCM*)-ωB97X-D/6-31+G(d,p)/ LANL2DZ level. The ωB97X-D functional has been parameterized to accurately take into account non-covalent interactions.[55] The effective core potential LANL2DZ[56] (Los Alamos National Laboratory 2 double-ζ) was used for nickel and the 6-31+G(d,p) basis set for carbon, nitrogen and hydrogen atoms. All calculations were carried out in implicit water solvent using the integral equation formalism variant of the polarizable continuum model (IEFPCM) since experiments were performed in aqueous solution. The Ni^{II}-**TImidP4** geometry was extrapolated from the crystalline structure of the porphyrin bis(imidazolium) salt (counter anions = BF_4^-) where the two imidazolium rings are fused to two neighboring pyrrolle units, similarly to previously reported for the parent bis(imidazole).[31] The optimization steps were performed within C_{2v} symmetry. Both singlet and triplet states have been considered. The triplet state is the most stable for Ni^{II}-**TMPyP4** metalloporphyrin; while the singlet state is the most stable for Ni^{II}-**TImidP4** metalloporphyrin. The energy differences ΔE between triplet and singlet states are -5.6 and 28.0 kcal.mol^{-1} for Ni^{II}-**TMPyP4** and Ni^{II}-**TImidP4** metalloporphyrins, respectively. The presence of close imidazolium moieties around the nickel-atom strongly affects porphyrin ligand field switching nickel state from triplet to singlet. Partial atomic charges were assigned using Antechamber programs after single point calculations at the aforesaid level of theory. Such calculations were carried out using Gaussian09 program.[57] Non-covalent parameters for the nickel-atom were derived from MCPB[58] (Metal Center Protein Builder) parameters included in AmberTools package.[59, 60] Porphyrin parameters are available in the ESI.

Molecular dynamics simulations. Solvated Tel22 G-quadruplex structures were obtained from PDB structures (anti-parallel structure with Na+, PDB ID: 143D; parallel structure with K+: 1KF1; Hybrid structure, PDB ID: 2HY9).[37,48, 61] The FF12SB force field as implemented in Amber12 package[60] was used to describe G-quadruplex structures. MD simulations were first performed on pure anti-parallel or parallel G-quadruplex structures. Water molecules were described as the "three-point" TIP3P model.[62, 63] The minimum distance between any atom of the system and the edge of the periodic box was set up at 15 Å. Water molecules were minimized prior to the entire system minimization. Boxes were thermally equilibrated by performing 50 ps heating MD simulation from 0 to 350 K. Then, 100 ps NPT MD simulations were carried out in order to obtain a solvent box density of 1 g.cm^{-3}. Finally, 100 ns NVT MD simulations were carried out. The equilibrated G-quadruplex parallel and anti-parallel structures were used for 1:1 metalloporphyrin – G-quadruplexes MD simulations. Five different binding modes were used as initial structures for 1:1 metalloporphyrin – anti-parallel/parallel G-quadruplex structures (Fig. 3). The same protocol was used to equilibrate 1:1 complex structures (*i.e.*, minimization, heating, and density equilibration). 100 ns MD simulations were then achieved in the (N,V,T) ensemble.

Binding free energy calculations. The MM-GBSA (molecular mechanics-Generalized Born surface area) script as implemented in Amber12 package was used to calculate the metalloporphyrin binding energies ($\Delta G_{binding}$). The internal contribution as well as non-covalent contributions were calculated using FF12SB and our own force field for G-quadruplexes and porphyrins, respectively (cut-off at 12 Å). The electrostatic solvation free energy was calculated by using the modified GB model in which effective Born radii are re-scaled to account for the interstitial space between atoms.[64, 65] The nonpolar contributions to solvation free energy were calculated using the linear combination of pairwise overlaps as implemented in Amber12 package. Although MM-GB/PBSA fails to accurately predict absolute binding free energy, it is a reliable approach to rank several binding modes involving similar systems. MM-GBSA has been shown to provide better results than MM-PBSA for this purpose.[66] Relative $\Delta\Delta G_{binding}$ are calculated with respect to the most stable structure for each 1:1 complex, being defined as $\Delta\Delta G_{binding} = 0$.

Acknowledgements

This work is supported by the Fonds de la Recherche Scientifique-FNRS (Belgium) under the grant n°2.4615.11-BINDER. J.R.-M. is FNRS post-doctoral researcher and M.S. is FNRS research associate. M.L. acknowledges SeRC (Swedish e-Science Research Center) for funding and FNRS for visiting professor position. P.N. and F.D.M. acknowledge financial support from the Swedish Research Council (Grant No. 621-2010-5014). The authors acknowledge SNIC (Swedish National Infrastructure for Computing) for providing computer resources. S.R., S.C. and M.Lo are grateful to the CNRS and the Agence Nationale de la Recherche (ANR) for financial support (research project ANR-09-JCJC-0089-01).

Notes and references

[a] Laboratory for Chemistry of Novel Materials, Center for Innovation in Materials and Polymers, University of Mons - UMONS, 20 Place du Parc, B-7000 Mons, Belgium. Tel: +32(0)65373868.
Email: mathieu.surin@umons.ac.be.
[b] Department of Physics, Chemistry and Biology (IFM) Linköping University, SE-581 83 Linköping, Sweden. Email: mathieu@ifm.liu.se.
[c] Institut Charles Gerhardt – UMR 5253, Université de Montpellier 2 - CC1701, Place Eugène Bataillon, F-34095 Montpellier Cedex 05, France. Email: sebastien.richeter@univ-montp2.fr.

† These authors contributed equally to this work.

Electronic Supplementary Information (ESI) available: Characterization of the compounds, supplementary UV-Vis and CD spectra, and computational data are available, see DOI: 10.1039/b000000x/

References

1. J. T. Davis and G. P. Spada, *Chem. Soc. Rev.*, 2007, **36**, 296-313.
2. O. Doluca, J. M. Withers and V. V. Filichev, *Chem. Rev.*, 2013, **113**, 3044-3083.
3. M. L. Bochman, K. Paeschke and V. A. Zakian, *Nat Rev Genet*, 2012, **13**, 770-780.
4. W. Fritzsche and L. Spindler Eds., *Guanine Quartets : Structure and Applications* Royal Society of Chemistry, 2013.

5. S. Rankin, A. P. Reszka, J. Huppert, M. Zloh, G. N. Parkinson, A. K. Todd, S. Ladame, S. Balasubramanian and S. Neidle, *J. Am. Chem. Soc.* , 2005, **127**, 10584-10589.
6. N. Maizels and L. T. Gray, *PLoS Genetics*, 2013, **9**, e1003468.
7. G. Biffi, D. Tannahill, J. McCafferty and S. Balasubramanian, *Nat. Chem.*, 2013, **5**, 182-186.
8. B. Maji and S. Bhattacharya, *Chem. Commun.*, 2014, **50**, 6422-6438.
9. Y. Wu and R. M. Brosh Jr, *FEBS Journal*, 2010, **277**, 3470-3488.
10. D. Monchaud and M. P. Teulade-Fichou, *Org. Biomol. Chem.*, 2008, **6**, 627-636.
11. S. Balasubramanian and S. Neidle, *Curr. Opin. Chem. Biol.*, 2009, **13**, 345-353.
12. W. O. Tucker, K. T. Shum and J. A. Tanner, *Curr. Pharm. Design*, 2012, **18**, 2014-2026.
13. G. W. Collie and G. N. Parkinson, *Chem. Soc. Rev.*, 2011, **40**, 5867-5892.
14. S. N. Georgiades, N. H. Abd Karim, K. Suntharalingam and R. Vilar, *Angew. Chem. Int. Ed.*, 2010, **49**, 4020-4034.
15. A. De Cian, E. DeLemos, J.-L. Mergny, M.-P. Teulade-Fichou and D. Monchaud, *J. Am. Chem. Soc.*, 2007, **129**, 1856-1857.
16. D. Monchaud, A. Granzhan, N. Saettel, A. Guédin, J. L. Mergny and M. P. Teulade-Fichou, *Journal of Nucleic Acids*, 2010, **vol. 2010**, Article ID 525862.
17. L. Wang, H. Wen, J. Liu, J. Zhou, C. Li and C. Wei, *Org. Biomol. Chem.*, 2011, **9**, 2648-2653.
18. J. K. Choi, G. Sargsyan, M. Shabbir-Hussain, A. E. Holmes and M. Balaz, *J. Phys. Chem. B*, 2011, **115**, 10182-10188.
19. M. Balaz, M. De Napoli, A. E. Holmes, A. Mammana, K. Nakanishi, N. Berova and R. Purrello, *Angew. Chem. Int. Ed.*, 2005, **44**, 4006-4009.
20. M. Balaz, K. Bitsch-Jensen, A. Mammana, G. A. Ellestad, K. Nakanishi and N. Berova, *Pure Appl. Chem.*, 2007, **79**, 801-809.
21. S. Ishihara, J. Labuta, W. Van Rossom, D. Ishikawa, K. Minami, J. P. Hill and K. Ariga, *Phys. Chem. Chem. Phys.*, 2014, **16**, 9713-9746.
22. G. Sargsyan, B. M. Leonard, J. Kubelka and M. Balaz, *Chem. Eur. J.*, 2014, **20**, 1878-1892.
23. R. F. Pasternack, *Chirality*, 2003, **15**, 329-332.
24. D. R. McMillin, A. H. Shelton, S. A. Bejune, P. E. Fanwick and R. K. Wall, *Coord. Chem. Rev.*, 2005, **249**, 1451-1459.
25. J. K. Choi, A. D'Urso and M. Balaz, *J. Inorg. Biochem.*, 2013, **127**, 1-6.
26. Y. Ikawa, S. Touden and Furuta, *Org. Biomol. Chem.*, 2011, **9**, 8068-8078.
27. C. Romera, O. Bombarde, R. Bonnet, D. Gomez, P. Dumy, P. Calsou, J. F. Gwan, J. H. Lin, E. Defrancq and G. Pratviel, *Biochimie*, 2011, **93**, 1310-1317.
28. T.-m. Ou, Y.-j. Lu, J.-h. Tan, Z.-s. Huang, K.-Y. Wong and L.-q. Gu, *ChemMedChem*, 2008, **3**, 690-713.
29. Q. Li, J. F. Xiang, H. Zhang and Y. L. Tang, *Curr. Pharm. Des.*, 2012, **18**, 1973-1983.
30. D. P. N. Goncalves, S. Ladame, S. Balasubramanian and J. K. M. Sanders, *Org. Biomol. Chem.*, 2006, **4**, 3337-3342.
31. M. Lo, J.-F. Lefebvre, D. Leclercq, A. van der Lee and S. Richeter, *Org. Lett.*, 2011, **13**, 3110-3113.
32. M. Lo, J.-F. Lefebvre, N. Marcotte, C. Tonnelé, D. Beljonne, R. Lazzaroni, S. Clément and S. Richeter, *Chem. Commun.*, 2012, **48**, 3460-3462.
33. J. Pan and S. Zhang, *J Biol Inorg Chem*, 2009, **14**, 401-407.
34. R. F. Pasternack, E. J. Gibbs and J. J. Villafranca, *Biochemistry*, 1983, **22**, 5409-5417.
35. J. Dai, M. Carver and D. Yang, *Biochimie*, 2008, **90**, 1172-1183.
36. K. W. Lim, S. Amrane, S. Bouaziz, W. Xu, Y. Mu, D. J. Patel, K. N. Luu and A. T. Phan, *J. Am. Chem. Soc.*, 2009, **131**, 4301-4309.
37. Y. Wang and D. J. Patel, *Structure*, 1993, **1**, 263-282.
38. A. T. Phan, *FEBS Journal*, 2010, **277**, 1107-1117.
39. A. Ambrus, D. Chen, J. Dai, T. Bialis, R. A. Jones and D. Yang, *Nucleic Acids Res.*, 2006, **34**, 2723-2735.
40. M. Bončina, J. Lah, I. Prislan and G. Vesnaver, *J. Am. Chem. Soc.*, 2012, **134**, 9657-9663.
41. J. Dai, C. Punchihewa, A. Ambrus, D. Chen, R. A. Jones and D. Yang, *Nucleic Acid Res.*, 2007, **35**, 2440-2450.
42. M. J. Morris, K. L. Wingate, J. Silwal, T. C. Leeper and S. Basu, *Nucl. Acids Res.* , 2012, **40**, 4137-4145.
43. M. Wieland and J. S. Hartig, *Angew. Chem. Int. Ed.*, 2006, **45**, 5875-5878.
44. P. Zhao, J. Z. Lu, F. Y. Hong, B. H. Ou, F. D. Zhang, L. N. Ma and H. M. Guo, *Spectrochim. Acta A*, 2013, **108**, 1-7.
45. A. De Cian, L. Guittat, M. Kaiser, B. Saccà, S. Amrane, A. Bourdoncle, P. Alberti, M.-P. Teulade-Fichou, L. Lacroix and J.-L. Mergny, *Methods*, 2007, **42**, 183-195.
46. D. Renčiuk, J. Zhou, L. Beaurepaire, A. Guédin, A. Bourdoncle and J.-L. Mergny, *Methods*, 2012, **57**, 122-128.
47. D. Monchaud, C. Allain, H. Bertrand, N. Smargiasso, F. Rosu, V. Gabelica, A. De Cian, J. L. Mergny and M. P. Teulade-Fichou, *Biochimie*, 2008, **90**, 1207-1223.
48. G. N. Parkinson, M. P. H. Lee and S. Neidle, *Nature*, 2002, **417**, 876-880.
49. C. J. Medforth, M. O. Senge, K. M. Smith, L. D. Sparks and J. A. Shelnutt, *J. Am. Chem. Soc.*, 1992, **114**, 9859-9869.
50. S. Rickling, L. Ghisdavu, F. Pierard, P. Gerbaux, M. Surin, P. Murat, E. Defrancq, C. Moucheron and A. Kirsch – De Mesmaeker, *Chem. Eur. J.*, 2010, **16**, 3951-3961.
51. X.-X. Huang, L.-N. Zhu, B. Wu, Y.-F. Huo, N.-N. Duan and D.-M. Kong, *Nucleic Acids Res.*, 2014, **42**, 8719-8731.
52. K. M. Kadish, D. Sazou, Y. M. Liu, A. Saoiabi, M. Ferhat and R. Guilard, *Inorg. Chem.*, 1988, **27**, 1198-1204.
53. M. C. Gomes, S. M. Woranovicz-Barreira, M. A. F. Faustino, R. Fernandes, M. G. P. M. S. Neves, A. C. Tome, N. C. M. Gomes, A. Almeida, J. A. S. Cavaleiro, A. Cunha and J. P. C. Tome, *Photochem. Photobiol. Sci.*, 2011, **10**, 1735-1743.
54. J. Wang, R. M. Wolf, J. W. Caldwell, P. A. Kollman and D. A. Case, *J. Comput. Chem.*, 2004, **25**, 1157-1174.
55. J.-D. Chai and M. Head-Gordon, *Phys. Chem. Chem. Phys.*, 2008, **10**, 6615-6620.
56. P. J. Hay and W. R. Wadt, *J. Chem. Phys*, 1985, **82**, 299-310.
57. M. J. Frisch, G. W. Trucks, H. B. Schlegel, G. E. Scuseria, M. A. Robb, J. R. Cheeseman, G. Scalmani, V. Barone, B. Mennucci, G. A. Petersson, H. Nakatsuji, M. Caricato, X. Li, H. P. Hratchian, A. F. Izmaylov, J. Bloino, G. Zheng, J. L. Sonnenberg, M. Hada, M. Ehara, K. Toyota, R. Fukuda, J. Hasegawa, M. Ishida, T. Nakajima, Y.

Honda, O. Kitao, H. Nakai, T. Vreven, J. A. Montgomery, J. E. Peralta, F. Ogliaro, M. Bearpark, J. J. Heyd, E. Brothers, K. N. Kudin, V. N. Staroverov, R. Kobayashi, J. Normand, K. Raghavachari, A. Rendell, J. C. Burant, S. S. Iyengar, J. Tomasi, M. Cossi, N. Rega, J. M. Millam, M. Klene, J. E. Knox, J. B. Cross, V. Bakken, C. Adamo, J. Jaramillo, R. Gomperts, R. E. Stratmann, O. Yazyev, A. J. Austin, R. Cammi, C. Pomelli, J. W. Ochterski, R. L. Martin, K. Morokuma, V. G. Zakrzewski, G. A. Voth, P. Salvador, J. J. Dannenberg, S. Dapprich, A. D. Daniels, Farkas, J. B. Foresman, J. V. Ortiz, J. Cioslowski and D. J. Fox, Wallingford CT, 2009.

58. M. B. Peters, Y. Yang, B. Wang, L. s. Füsti-Molnár, M. N. Weaver and K. M. Merz, *J. Chem. Theory Comput.*, 2010, **6**, 2935-2947.
59. R. Salomon-Ferrer, D. A. Case and R. C. Walker, *Wiley Interdisciplinary Reviews: Computational Molecular Science*, 2013, **3**, 198-210.
60. D. A. Case, T. A. Darden, T. E. Cheatham, C. L. Simmerling, J. Wang, R. E. Duke, R. Luo, R. C. Walker, W. Zhang, K. M. Merz, B. Roberts, S. Hayik, A. Roitberg, G. Seabra, J. Swails, A. W. Götz, I. Kolossváry, K. F. Wong, F. Paesani, J. Vanicek, R. M. Wolf, J. Liu, X. Wu, S. R. Brozell, T. Steinbrecher, H. Gohlke, Q. Cai, X. Ye, J. Wang, M.-J. Hsieh, G. Cui, D. R. Roe, D. H. Mathews, M. G. Seetin, R. Salomon-Ferrer, C. Sagui, V. Babin, T. Luchko, S. Gusarov, A. Kovalenko and P. A. Kollman, *AMBER 12*, (2012), University of California, San Francisco.
61. S. Burge, G. N. Parkinson, P. Hazel, A. K. Todd and S. Neidle, *Nucleic Acids Res.*, 2006, **34**, 5402-5415.
62. W. L. Jorgensen, J. Chandrasekhar, J. D. Madura, R. W. Impey and M. L. Klein, *J. Chem. Phys*, 1983, **79**, 926-935.
63. D. J. Price and C. L. Brooks, *J. Chem. Phys*, 2004, **121**, 10096-10103.
64. A. Onufriev, D. Bashford and D. A. Case, *J. Phys. Chem. B*, 2000, **104**, 3712-3720.
65. A. Onufriev, D. Bashford and D. A. Case, *Proteins: Struct., Funct., Bioinf.*, 2004, **55**, 383-394.
66. T. Hou, J. Wang, Y. Li and W. Wang, *J. Chem. Inf. Model.*, 2010, **51**, 69-82.